

On the Characterization of Buried Targets Under a Rough Surface Using the Wigner–Ville Transformation

Octavien Cmielewski, Marc Saillard, *Member, IEEE*, Kamal Belkebir, and Hervé Tortel

Abstract—This letter considers the problem of detecting and characterizing a target buried beneath a rough surface separating two homogeneous half spaces. The problem of detecting the target is tackled by analyzing the frequency-averaged Wigner–Ville function, the purpose of which is to filter out rough surface scattering. Characterization of the target is performed using the iterative solution derived from the Newton–Kantorovitch algorithm as applied to the Wigner–Ville function instead of the scattered field as is usually done. In addition, the scattering model involved in the inversion scheme assumes a flat interface, and surface roughness is handled as clutter. The efficiency of the approach is illustrated through numerical experiments, and the comparison between inversions from the scattered field and the Wigner–Ville function is reported.

Index Terms—Buried object detection, electromagnetic scattering, electromagnetic tomography, imaging, inverse problems, rough surfaces, Wigner–Ville transform.

I. INTRODUCTION

THIS LETTER focuses on the problem of detection and characterization of an object buried at low depth below a rough surface from multifrequency multistatic data recorded along a segment of line above the interface. This problem has been recently addressed in [1] and [2], where the surface scattering contribution is included in the inversion procedure, thus leading to the reconstruction of both the surface profile and the target. However, clutter rejection based on signal processing techniques under the guidance of simple physics models [3], [4] is much less time consuming than completely characterizing the clutter through global inversion of the exact wave equation. In addition, clutter rejection is required for the detection of the target, which has to be performed prior to applying inversion algorithms restricted to small areas. This preliminary step has been skipped in [1] and [2]. A great variety of signal processing techniques are devoted to the detection of deterministic signals polluted by random noise for various kinds of noise and applications. Physics-based models are useful to design a well-suited detector in the sense that they provide physical interpretation in terms of interference. Here, analytical calculations performed in the frame of a low-frequency approximation have led us to

propose an algorithm based on the Wigner–Ville transform. Additional summations over various frequencies aim at damping the clutter contribution as if an ensemble average over many surface samples was performed.

If an efficient detector is built from the data, an inversion algorithm based on it should also be robust against clutter if an accurate forward solver for the actual problem without clutter is available. This is investigated here, where inversion of the Wigner–Ville transform is performed under the assumption of a flat interface, i.e., considering surface roughness contribution as noise.

II. DETECTION

In this problem, detection is a matter of competition between surface and subsurface scattering. It is assumed that the buried object is at such a low depth that time gating does not permit us to separate the two contributions. The most popular technique in the radar community is synthetic aperture radar (SAR) processing, which only requires the backscattered field. However, SAR processing is not robust against clutter and is probably not optimal for a multistatic configuration. Indeed, it is assumed here that both the transmitter and the receiver can move along a portion of line above the interface, at $y = y_0$. Our aim is thus to build a detector, robust against surface scattering, which takes benefit from the multistatic configuration and that lies on data only. Such a problem has been investigated in a far-field configuration [5], [6], but has to be revisited in a near-field configuration, since surface scattering does not present any privileged direction in this latter case.

In the following, investigation is restricted to cylindrical geometries, with electric fields parallel to the direction of invariance (TM polarization). The transmitters are two-dimensional (2-D) electric dipoles radiating an isotropic cylindrical wave. f , k_0 , and k are the frequency and wavenumbers in the upper and lower media, respectively. If $E_f^s(x, x_0)$ denotes the scattered electric field recorded at (x, y_0) when the transmitter is located at (x_0, y_0) , correlating the scattered fields recorded at $x + x'$ and $x - x'$ and integrating with respect to x' and x_0 lead to

$$W_f(x) = \int \int E_f^s(x + x', x_0) \cdot \overline{E_f^s(x - x', x_0)} dx' dx_0 \quad (1)$$

where the over bar denotes the complex conjugation. Forgetting the integration over x_0 , this quantity can be seen either as the restriction to the x axis of the Wigner–Ville transformation [7]

Manuscript received September 20, 2005; revised January 13, 2006.

O. Cmielewski, K. Belkebir, and H. Tortel are with the Institut Fresnel, UMR-CNRS 6133, Université Paul Cézanne Aix-Marseille III, Université de Provence Aix-Marseille I, 20 13397 Marseille Cedex, France (e-mail: kamal.belkebir@fresnel.fr).

M. Saillard is with the Laboratoire de Sondages Electromagnetiques de l'Environnement Terrestre, UMR-CNRS 6017, Université du Sud Toulon Var, 83957 La Garde Cedex, France.

Digital Object Identifier 10.1109/LGRS.2006.874165

or as the angular correlation function if the transmitter and receivers are moved to the far field. In the following, $W_f(x)$ will be referred to as the Wigner–Ville function. It must be pointed out that integrating with respect to x_0 is not just a way of performing some kind of ensemble average to smooth the surface roughness contribution. Indeed, considering a small scatterer located at x_t and at depth d below a flat interface, analytical calculations show that the contribution X_{tp} to (1) coming from the combination of the specular reflection at $x + x'$ with target scattering at $x - x'$ provides a peak when x coincides with x_t if integration with respect to x_0 is performed [8], since it writes as

$$X_{\text{tp}}(x) \simeq \int_{-k_0}^{k_0} F(\alpha) \exp(-2i\gamma d) \exp(2i\alpha(x - x_t)) d\alpha \quad (2)$$

where $F(\alpha)$ is the ratio of two polynomial functions of α , $\gamma_0 = \sqrt{k_0^2 - \alpha^2}$, and $\gamma = \sqrt{k^2 - \alpha^2}$ and is proportional to the scattering amplitude of the target. If kd is small, $\exp(-2i\gamma d)$ has almost no influence and a peak at $x = x_t$ results from the presence of $\exp(2i\alpha(x - x_t))$ in the integral.

The expectation is that when the surface roughness is superimposed, its contributions at $x + x'$ and $x - x'$ are not correlated. Obviously, this is related to the characteristics of the surface profile. A deep investigation of the performance of such a detector has been achieved in [8], where it has been shown that performance deteriorates with increasing roughness height but is almost independent of the correlation length. This leads us to operate in the low frequency range, with a compromise between clutter reduction and requirements for target detection and characterization. In this range, surface roughness contribution can be estimated with the first-order small perturbation theory. As a result, the clutter contribution to W_f , which competes with X_{tp} , is proportional to surface height h .

It has also been observed that the performance of the detector depends on the frequency via $\exp(-2i\gamma d)$ in (2) and that the optimal frequency for detection not only varies from one surface sample to the other but is also strongly dependent on the permittivity of the lower medium, which, in general, is not known. To ensure that the optimal frequency band is included in the process, averaging of the Wigner–Ville function is thus performed over a wide frequency range. In addition, such a procedure also allows one to smooth the surface roughness contribution. If the frequency gap between two successive frequencies is large enough, the scattered fields are uncorrelated and this can be seen as some kind of ensemble average.

III. INVERSION

Synthetic data are provided by the forward solver described in [10], which accurately takes surface roughness into account thanks to a rigorous boundary integral formalism. For the inversion, a domain integral representation of the fields with a flat interface is used, preventing any “inverse crime.” The same iterative inversion scheme has been applied to both data sets, scattered field and Wigner–Ville function. It is based on the Newton–Kantorovitch (NK) algorithm [11], [12]. Details on

the numerical implementation will be reported elsewhere. Just the general principle is given below.

For sake of simplicity, let us schematize the forward problem with an operator \mathbf{O} , linking the data g (scattered field or Wigner–Ville function) to the permittivity contrast $\chi(x, y) = \varepsilon_r(x, y) - \varepsilon_{br}$, where ε_{br} and $\varepsilon_r(x, y)$ denote the permittivity of the background medium and the permittivity at (x, y) , respectively, i.e.,

$$g = \mathbf{O}\chi. \quad (3)$$

The inverse problem is stated as determining the contrast distribution in a bounded domain Ω such that the data g , computed from (3), match the input data g^{input} . The NK method iteratively builds up the solution to (3) by successively solving the direct problem and a local linear inverse problem. At each iteration step, an estimation of the contrast function χ is given by

$$\chi_n = \chi_{n-1} + \delta\chi \quad (4)$$

where $\delta\chi$ is a correction obtained by solving (least square sense) the linear system

$$[\mathbf{D}^\dagger \mathbf{D} + \mu^2 \mathbf{I}] \delta\chi = \mathbf{D}^\dagger (g - g^{\text{input}}) \quad (5)$$

with \mathbf{D} being the Fréchet derivative of \mathbf{O} , \mathbf{D}^\dagger the adjoint of \mathbf{D} , \mathbf{I} the unit matrix, and μ^2 a positive real parameter. In (5), a zeroth-order Tikhonov regularization is used [13]. The regularization parameter μ^2 changes during the iterative process according to the values of the condition number of D . All the reported reconstructions, from either scattered fields or Wigner–Ville transforms, were carried out with inversion of data for all frequencies at the same time. We did not apply the frequency-hopping approach [14].

IV. NUMERICAL EXPERIMENTS

For sake of simplicity, we restrict ourselves to purely dielectric materials. Consequently, in the inversion algorithms, a real contrast χ is enforced. Our aim is not to give statistical results here, but various samples of rough surfaces have been considered and some relevant trends have been noticed when comparing inversion based on scattered field and the Wigner–Ville function. In the first part of this section, such a comparison has been achieved for the configuration depicted in Fig. 1 for various roughness heights. The end of the section focuses on the ability of the method to determine the orientation of the target. This is investigated by considering the same rectangular target as depicted in Fig. 1 but tilted of an angle of -30° .

The configuration under study involves an interface separating two semi-infinite media, with dielectric constants $\varepsilon_r = 1$ (air) above and $\varepsilon_r = 5$ (dry soil) below. A rectangular cross-sectional dielectric target is buried in the soil. The dimensions of the target under test along the x and y directions are $l_x = 7.8$ and $l_y = 3.2$ cm, respectively. The relative permittivity of the scatterer is $\varepsilon_r = 2$ and is buried at a depth of $d = 5$ cm (distance is measured from the interface to the center of the target). The measurement line Γ of length 60 cm is located

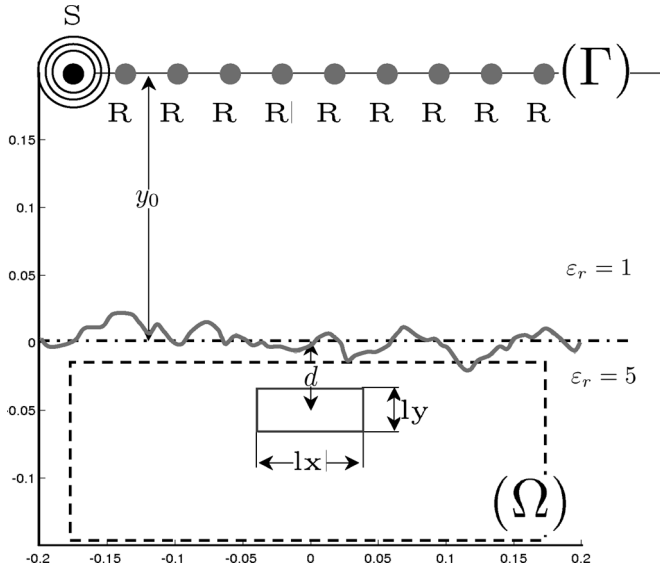


Fig. 1. Configuration of the studied problem. A deterministic target confined in bounded-box Ω is buried under a rough surface at depth h . Transmitting antennas moving along a segment of line Γ located at distance d from the interface illuminate the target and receiving antennas measure the scattered field. The target under test is a rectangular cylinder of dimension $l_x \times l_y$.

in the air at a distance of $y_0 = 20$ cm. $N_a = 21$ transmitting and receiving antennas are evenly distributed along Γ . Furthermore, Γ moves along the x axis over a distance of 60 cm by steps of 3 cm. Thus, one can compute for each frequency a Wigner–Ville function from (1) sampled in 21 positions along the x axis.

We have considered typical parameters of soil surface roughness, as described in [9]. The examples studied throughout this paper deal with a sample of a rough surface with exponential correlation function, 3.3 cm correlation length, and 1 cm rms height. The Wigner–Ville function has been averaged over seven operating frequencies in the range of 400–1600 MHz.

In Fig. 2, the sum over the frequencies of the Wigner–Ville function has been plotted for (a) the target under a flat interface, (b) without target but surface roughness, and (c) the target under the rough surface. Clearly, the last curve combines the first two ones, and the contribution of the target to $W(x) = \sum_f W_f(x)$ is much larger than it is to the scattered field.

In all reported results of the inversions, the same initial guess is considered for both inversions (from scattered fields and from Wigner–Ville transforms). This is motivated by our wish to compare both methods. The initial guess is zero-valued contrast. This corresponds to no presence of targets in the investigated domain. Another choice, based on a back-propagation technique [12], is possible when data are scattered fields. However, this choice needs to be revisited when dealing with Wigner–Ville transforms. The regularization parameter is chosen to ensure invariance of the condition number of D during the inversion process since we have noticed a direct link between the rms height h and the appropriate condition number. We have proceeded as follows. Let us assume that the condition number CN ensures a good compromise between speed of convergence and resolution at $h = 0.33$ cm. If the same CN is used for $h = 0.66$ cm, the algorithm is no longer

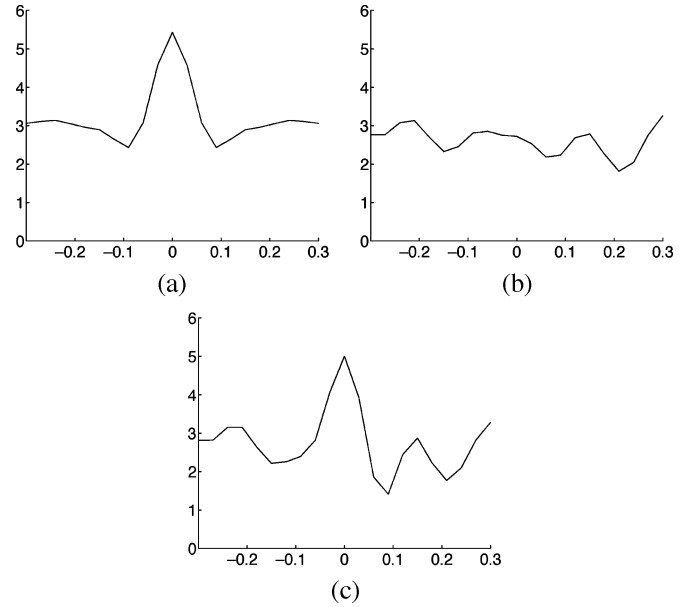


Fig. 2. Wigner function for (a) target under a flat interface, (b) without target but surface roughness, and (c) target under the rough surface. The rms height of the surface is $h = 1$ cm.

converging or converges very slowly. Decreasing CN permits to speed up the convergence, and we have noticed that keeping the product $h \cdot \text{CN}$ constant ensures similar speed of convergence for the various rms heights considered here. For the present example, $\text{CN} = 10$ for $h = 1$ cm, $\text{CN} = 15$ for $h = 0.66$ cm, and $\text{CN} = 30$ for $h = 0.33$ cm. Obviously, reducing the condition number restricts the potential of the inversion algorithm, and, in the present case, at $h = 1$ cm, the cost function is only reduced by a factor of 5 from initial guess to convergence. Therefore, this approach becomes questionable for stronger clutter.

Results of the inversion of the rectangular target plotted in Fig. 3 correspond to the fourth iterate. We did not observe any marked changes when continuing iterating. We also noticed that the smallest final value (fourth iteration step) of the cost function is in all cases obtained with Wigner–Ville transforms.

To quantify the robustness of the inversion against clutter, we have computed the L_2 norm of the difference between the reconstructed maps of permittivity with and without surface roughness, normalized by the map associated with the flat interface. When the rms height reaches 1 cm, one gets 1.1 for the Wigner–Ville function and 2.3 for the scattered field. The ratio of these errors is almost constant (close to 0.5) for this range of roughness parameters. In fact, it is the same as the ratio derived from the true permittivity. Inversion thus keeps it almost unchanged.

We have also counted the number of pixels outside the range supposed to represent the background, $\varepsilon_r = 5 \pm 1$. Fig. 3 shows the corresponding maps, with domain Ω 28 cm wide and 11 cm high, with an upper boundary at 1.6 cm (2 pixels) below the mean elevation of the interface. The influence of surface roughness height was investigated with 0.33-cm steps. The upper figures correspond to flat interface and the target clearly appears. An rms of 0.33 cm is very similar, and hence, not plotted. For an rms height of 0.66 cm, 36 and 71 pixels

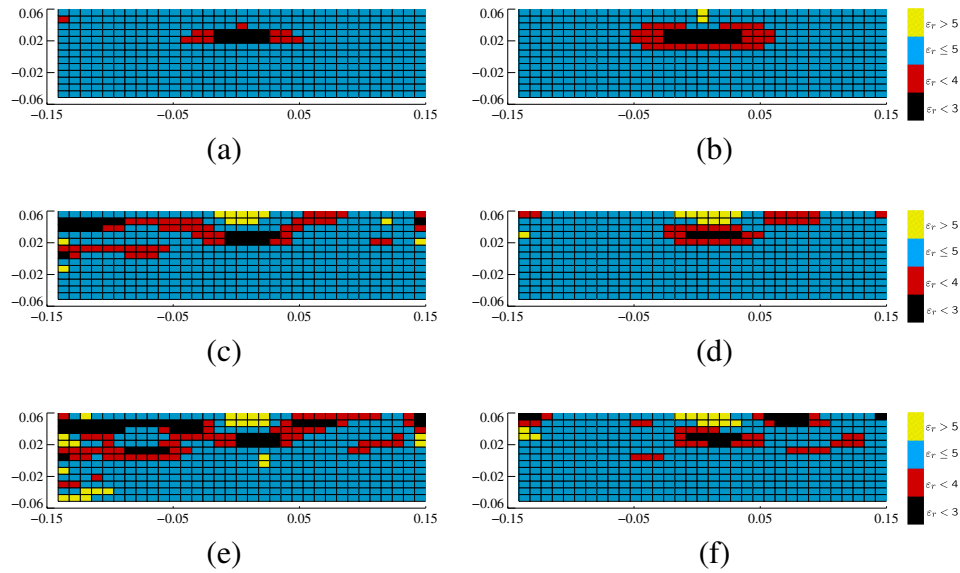


Fig. 3. Reconstructed relative permittivity (real part) using the scattered field (modulus and phase, left column) and using Wigner–Ville function (right column). First row shows that the interface is flat; second row with rough interface (rms height = 6.6 mm); third row with rms height = 10 mm.

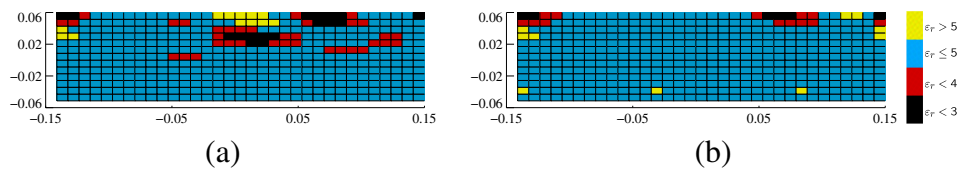


Fig. 4. Reconstructed relative permittivity (real part) using Wigner–Ville function. (a) Same as Fig. 3(f). (b) Same as (a) without buried object.

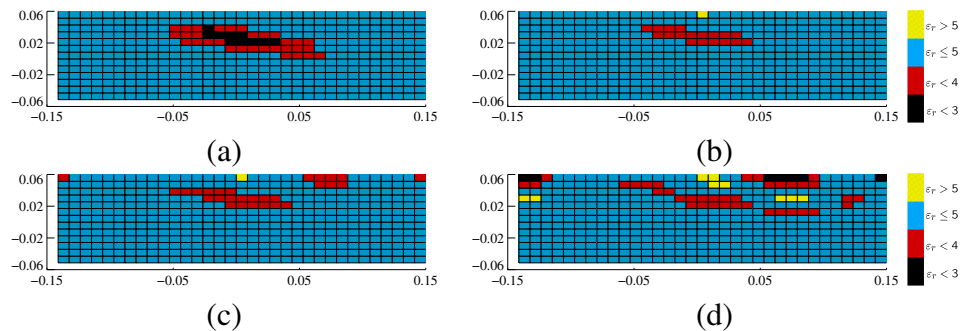


Fig. 5. Reconstructed relative permittivity (real part) using the Wigner–Ville function. The target under test is the same as in Fig. 3 but tilted at -30° . (a) Flat interface. (b) Rough interface (rms height 3.3 mm). (c) RMS height 6.6. (d) RMS height 10.

(among 429) were found smaller than the lower boundary with Wigner–Ville and field-based approaches, respectively, with 23 and 20 located on the support of the target. Regarding the upper boundary, 10 and 12 pixels were found with higher permittivity in the maps, mainly located above the target, since reconstruction in a stratified geometry often leads to vertically oscillating permittivity profiles [15], even though a multifrequency approach is used here. Therefore, 13 and 51 pixels may contribute to false alarm, translating in a quantitative way the improvement of robustness brought by the Wigner–Ville function, as suggested when looking at Fig. 3. In addition, since erroneous pixels are mainly concentrated in the vicinity of the surface, the probability of detection rapidly decreases as their number increases. When the height is increased up to 1 cm,

the difference between the two approaches becomes even more clear. It can be noticed that erroneous pixels appear at the corners of the domain Ω to mimic the contribution of the surface that is located outside Ω .

In Fig. 3(d) and (f), it seems that two dielectric objects with negative contrast are buried below the rough surface, too close to each other to be separated by the Wigner–Ville function (Fig. 2 exhibits a single peak) but separable when multiple scattering is taken into account by the inversion algorithm. To understand the origin of this spurious object, located around $x = 7$ cm, inversion was also performed without any buried scatterer under the rough surface. Fig. 4(b) still exhibits pixels with negative contrast at the same location, but a smaller number with smaller contrast in average, as compared with

Fig. 4(a). This shows that the interaction between the target and the interface has enhanced the signature of clutter.

The results mentioned above clearly show the interest to use the Wigner–Ville transform rather than the scattered fields (modulus and phase). Consequently, in what follows, only reconstructions obtained from Wigner–Ville transforms are presented. We focus our study on the ability to determine the orientation of the previous target in the presence of surface clutter. To this end, the same object is tilted of an angle of -30° with respect to the horizontal axis. Other parameters (permittivity, position, operating frequencies, etc.) of the configuration under test remain unchanged. Fig. 5 shows the results of the inversion using Wigner–Ville transforms for various values of the rms height of the surface. Clearly, the orientation as well as the support of the target is well retrieved up to an rms height of 0.66 cm. It should be noted that the spurious object around $x = 7$ cm still appears in Fig. 5(c) and (d). This confirms the interpretation developed previously, i.e., interactions between the target and the surface also contribute to the spurious object.

V. CONCLUSION

To roughly sum up, we have tried to show that when strong clutter occurs, “what is helpful for detection is also helpful for inversion.” To this end, since the Wigner–Ville function provides a robust means of detecting an object buried at low depth below a rough surface, optimization was performed with respect to it and compared with standard inversion based on optimization of the scattered field. Although this function only provides N real data, it leads to a more robust algorithm than the same inversion method as applied to the N^2 complex fields from which it is derived. This is clearly illustrated in the letter where it is tested against a rather realistic configuration. In our opinion, the approach suggested here has just only touched the topic and, with no doubt, can be improved.

REFERENCES

- [1] V. Galdi, H. Feng, D. A. Castanon, W. C. Carl, and L. B. Felsen, “Moderately rough surface underground imaging via short-pulse quasi-ray Gaussian beams,” *IEEE Trans. Antennas Propagat.*, vol. 51, no. 9, pp. 2304–2317, Sep. 2003.
- [2] I. Catapano, L. Crocco, and T. Isernia, “A simple two-dimensional inversion technique for imaging homogeneous targets in stratified media,” *Radio Sci.*, vol. 39, no. 1, p. RS1012, Feb. 2004.
- [3] T. Dogaru, L. Collins, and L. Carin, “Optimal time-domain detection of a deterministic target buried under a randomly rough interface,” *IEEE Trans. Antennas Propagat.*, vol. 49, no. 3, pp. 313–326, Mar. 2001.
- [4] C. Rappaport, M. El-Shenawee, and H. Zhan, “Suppressing GPR clutter from randomly rough ground surfaces to enhance nonmetallic mine detection,” *Subsurf. Sens. Technol. Appl.*, vol. 4, no. 4, pp. 311–326, 2003.
- [5] G. Zhang, L. Tsang, and Y. Kuga, “Studies of the angular correlation function of scattering by random rough surfaces with and without a buried object,” *IEEE Trans. Geosci. Remote Sens.*, vol. 35, no. 2, pp. 444–453, Mar. 1997.
- [6] G. Zhang and L. Tsang, “Application of angular correlation function of clutter scattering and correlation imaging in target detection,” *IEEE Trans. Geosci. Remote Sens.*, vol. 36, no. 5, pp. 1485–1493, Sep. 1998.
- [7] P. Flandrin, *Time–Frequency/Time–Scale Analysis*. New York: Academic, Sep. 1998.
- [8] O. Cmielewski, “Détection d’objets enfouis sous des interfaces rugueuses,” Ph.D. dissertation, Inst. Fresnel, Univ. Provence, Marseille, France, Nov. 2005.
- [9] Y. Oh, K. Sarabandi, and F. T. Ulaby, “An empirical model and an inversion technique for radar scattering from bare soil surfaces,” *IEEE Trans. Geosci. Remote Sens.*, vol. 30, no. 2, pp. 370–381, Mar. 1992.
- [10] M. Saillard and G. Toso, “Electromagnetic scattering from bounded or infinite subsurface bodies,” *Radio Sci.*, vol. 32, no. 4, pp. 1347–1359, 1997.
- [11] A. Roger, “Newton–Kantorovitch algorithm applied to an electromagnetic inverse problem,” *IEEE Trans. Antennas Propagat.*, vol. AP-29, no. 2, pp. 232–238, Mar. 1981.
- [12] K. Belkebir, R. E. Kleinman, and C. Pichot, “Microwave imaging—Location and shape reconstruction from multifrequency scattering data,” *IEEE Trans. Microw. Theory Tech.*, vol. 45, no. 4, pp. 469–476, Apr. 1997.
- [13] A. N. Tikhonov and V. Y. Arsenin, *Solution of Ill-Posed Problems*. Washington, DC: Weston V. H., 1977.
- [14] A. G. Tijhuis, K. Belkebir, A. C. S. Litman, and A. P. de Hon, “Theoretical and computational aspects of 2-D inverse profiling,” *IEEE Trans. Geosci. Remote Sens.*, vol. 39, no. 6, pp. 1316–1330, Jun. 2001.
- [15] A. Dubois, K. Belkebir, and M. Saillard, “Localization and characterization of two-dimensional targets buried in a cluttered environment,” *Inv. Probl.*, vol. 20, no. 6, pp. S63–S79, 2004.